IONIZED BUBBLES IN THE PRIMORDIAL UNIVERSE

Juan Antonio Molina Calzada
Internship in CAB

IONIZED BUBBLES IN THE PRIMORDIAL UNIVERSE

Juan Antonio Molina Calzada
Internship in Centro de Astrobiología (CAB), Master in Astrophysics
Faculty of Physics, Universidad Complutense de Madrid
Supervisor: Miguel Mas Hesse
Version: May 2024

Contents

1 Introduction

The epoch of reionization was a cosmological period between redshift $6 < z < 20$, during which the first generations of Population III stars and galaxies emitted radiation that reionized the Universe.

The formation of massive stars (O and B stars) generates regions of ionized hydrogen, known as HII regions, which emit characteristic lines in different series of hydrogen. The Balmer series produces emissions in the optical range, while the Lyman series generates emissions in the ultraviolet, with the Lyman alpha line (Lyα) being the most intense at 1216 Å. This emission allows us to estimate the number of ionizing photons and, consequently, the number of massive stars formed (Gazagnes et al., 2020). Furthermore, due to its wavelength, Lyα is detectable from ground-based telescopes in the visible range for galaxies with redshifts between ∼2 and ∼5, and even in the infrared for higher redshifts.

Lyα emission faces a crucial challenge due to its resonant nature. When Lyα photons pass through a cloud of neutral hydrogen (HI), they are absorbed and reemitted repeatedly in all directions due to resonant scattering (Madau, 1995). Additionally, the mean free path of the photons is considerably lengthened, increasing the probability of destructive interactions even with minimal amounts of dust (Hayes et al., 2011). As a result, the presence of HI in front of a star-forming galaxy not only inhibits the detection of Lyα emission but also makes it observable in absorption. Only in cases where HI is in motion, relative to the HII gas, is it possible to detect a fraction of the Lyα emission line. While one might consider using Hα instead of the Lyα line, at such high redshifts, this line is redshifted to wavelengths above 5 microns, making its detection extremely challenging. However, new space telescopes such as the JWST are enabling the first studies (Williams et al., 2023) using this emission instead.

An area of current research relevance is understanding the events and timing of the reionization of the intergalactic medium (IGM). The predominant hypothesis posits that the IGM was initially in a neutral state but was eventually reionized by an abundant amount of ionizing photons from primordial galaxies undergoing intense episodes of massive star formation. This reionization process is estimated to have been completed at a redshift of $z \sim 6$, after starting around a redshift of $z \sim 20$, coinciding with the emergence of the first massive stars in primordial galaxies (Robertson et al., 2010).

This reionization process propagated through bubbles and superbubbles of ionized material surrounding galaxies where the most intense processes of massive star formation occurred. By a redshift of approximately 6, these bubbles had already overlapped, making most of the IGM predominantly ionized. Although colder and isolated neutral clouds could still exist.

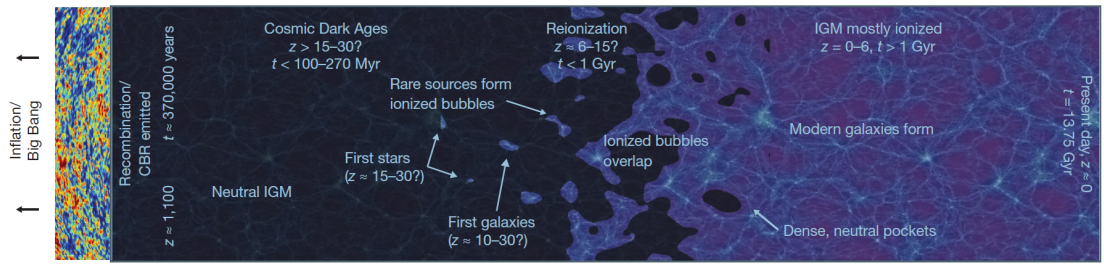

Figure 1: Diagram of the reionization process. Around $z \sim 20$, the reionization epoch begins, during which the first ionized bubbles form. These bubbles continue to form and grow in size until they overlap with their neighbors, thus occupying the entire intergalactic medium around $z \sim 6$. Figure extracted from Robertson et al. (2010).

The Lyα emission stands out as one of the most prominent tracers, practically the only one, of the formation of massive stars in primordial galaxies, as well as their ability to generate ionized bubbles in their surroundings. However, because much of the IGM is still in a neutral state at these redshifts, Lyα photons emitted from these bubbles would experience resonant scattering and would not be detected (Mason and Gronke, 2020). Despite this, it is observed that, while from a redshift greater than $\sim$7, the number of galaxies with Lyα emission (LAEs: Lyman Alpha Emitters) decreases significantly, a considerable number is still recorded (Pentericci et al., 2009). It is postulated that this phenomenon can be explained by the sufficiently large size of the ionized bubbles, which causes a difference in the recession velocity between the neutral edges of the bubble (due to the expansion of the Universe) and the star-forming galaxies. This disparity in redshifts would result in the Lyα photons not being at the exact wavelength of 1216 Å in the frame of IGM, thus avoiding resonant scattering and allowing their passage through the IGM to reach us. To understand this process well, it is necessary to estimate the size of these bubbles and verify if they would be large enough for the Hubble flow to allow the passage of Lyα photons (Mas-Hesse et al., 2003).

The sections of this work will proceed as follows. In Section 2, we will outline the objectives of this work and why determining the size of ionizing bubbles is important. In Section 3, we will introduce the different methods for estimating the size of ionized bubbles. We will also explain the Sobral relation. In Section 4, we will present the different samples of galaxies we will work with and the derivation of some of their parameters. In Section 5, we will explain and apply the different models to calculate escape fractions, as well as compare and analyze the calculated bubble sizes. Finally, in Section 5, we will summarize the most important results and the upcoming advancements in this field of astrophysics.

2 Objectives

The study of star formation processes in the early epochs of the Universe requires the detection of recombination lines emitted by galaxies at high redshifts. Currently, detecting these lines poses a challenge. Due to the expansion of the Universe, the detected recombination lines have undergone a sufficiently high redshift to make them difficult to detect with current instruments. Although the recent JWST telescope can detect the Hα recombination line at high redshifts, the Lyα line has been and continues to be the most used for studying these objects. Its wavelength in the UV allows it to be detected in the IR from Earth at high redshifts.

The detection of the Lyα line is of particular interest for studying star formation processes at high redshifts. However, as we have already mentioned in the introduction, this line is affected by absorption and scattering processes when passing through a region of neutral hydrogen. Nonetheless, estimating the size of the ionized bubbles surrounding galaxies at high redshifts is of great importance because if they are large enough, these Lyα emissions can escape and be detected from Earth. If the bubble is not sufficiently large, this emission will be attenuated, thus detecting only a fraction of it. Using observed Lyα emissions without considering the escape fractions can lead to erroneous statistics.

Knowing the fraction of Lyman alpha photon escape will allow a detailed study of star formation processes in galaxies at high redshifts. To do this, it is crucial to estimate the size of the ionized bubble, which is the aim of this work.

3 Strömgren radius estimation

A Strömgren sphere (Strömgren, 1939) is an ionized hydrogen (HII) sphere around a hot star of the O-B spectral class produced by the ionizing photons.

Very hot stars of spectral classes O or B emit highly energetic radiation, particularly ultraviolet, capable of ionizing neutral hydrogen (HI) in the surrounding interstellar medium, causing hydrogen atoms to lose electrons and form HII. Eventually, free electrons recombine with hydrogen ions, emitting energy as a series of photons of decreasing energy. These photons lose energy as they move away from the star, becoming insufficient for further ionization. The concept of a Strömgren sphere describes these ionized regions theoretically, preventing the entire interstellar medium from being ionized. This concept can be extrapolated to the large ionized bubbles formed around galaxies, when a significant fraction of the ionizing photons they emit are able to escape to the intergalactic medium.

One of the main goals of interstellar and intergalactic medium physics is to estimate the radius of these Strömgren spheres. To achieve this, some simple models assume an equilibrium between the number of photoionizations and recombinations and more complex models take into account the evolution of the size of the bubble with time (Rodríguez Espinosa et al., 2021). In this study, we will analyze a first model that assumes equilibrium and another more complex model called the Yajima model (Yajima et al., 2018).

3.1 Strömgren sphere in equilibrium

Firstly, we will derive the expression to estimate the Strömgren radius assuming equilibrium between ionizations and recombinations, R_s^{eq}. The equation from which is derived, introduced by Cen and Haiman (2000), is given by

$$\frac{d(R_s^{eq})^3}{dt} = 3H(z)(R_s^{eq})^3 + \frac{3\dot{N}_{ion}}{4\pi < n_H >} - C_H < n_H > \alpha_B (R_s^{eq})^3 . \tag{1}$$

Here, we break down the equation's components: the first term accounts for the expansion of the Universe, the second term represents ionization, and the third term denotes recombinations. Specifically, $H(z)$ is the Hubble parameter, n_H is the hydrogen density, and C_H is a constant, all of which are dependent on redshift z as well. The parameter α_B represents the recombination factor, which, assuming an electronic temperature of $T_e = 10^4 K$, has a value of $\alpha_B = 8.8 \times 10^{-13} (pMpc)^3 \cdot s^{-1}$. Finally, N_{ion} is the number of ionizing continuum photons emitted per second.

Even if there is an equilibrium between photons and recombinations, the physical volume can still increase due to the expansion of the Universe. Thus we need to require that the volume does not vary with the expansion, i.e., if the source of photons is constant the comoving volume of the bubble is constant. This comoving volume is given by

$$V_C = \frac{4\pi}{3} \cdot \frac{(R_s^{eq})^3}{a^3}, \tag{2}$$

where a is the Universe scale factor. Substituting the equation 2 in equation 1 and deriving, we get the Strömgren radius in proper distance ($pMpc$).

$$R_s^{eq}[pMpc] = \left(\frac{\dot{N}_{ion}}{4\pi C_H < n_H >^2 \alpha_B} \right)^{1/3} . \tag{3}$$

This is the equation that gives the radius of an ionized bubble in equilibrium between the number of ionizing photons emitted and the number of recombinations. It is in fact an equation that can be seen in Spitzer (1978), and Osterbrock (1989), albeit with different symbols. It is important to note that this relation only provides an upper bound on the size of the ionized bubble since we are assuming equilibrium.

Note that, to convert the Strömgren radius to comoving distances ($cMpc$) you only have to multiply the result in $pMpc$ by $(1+z)$.

3.2 Yajima model

Another way to estimate the Strömgren radius, but without assuming equilibrium, is what is proposed in the Yajima model (Yajima et al., 2018). This model establishes a relation between the observed Lyman alpha line luminosity and the Strömgren radius (in proper distance) for different redshifts. This relationship is depicted in Figure 2.

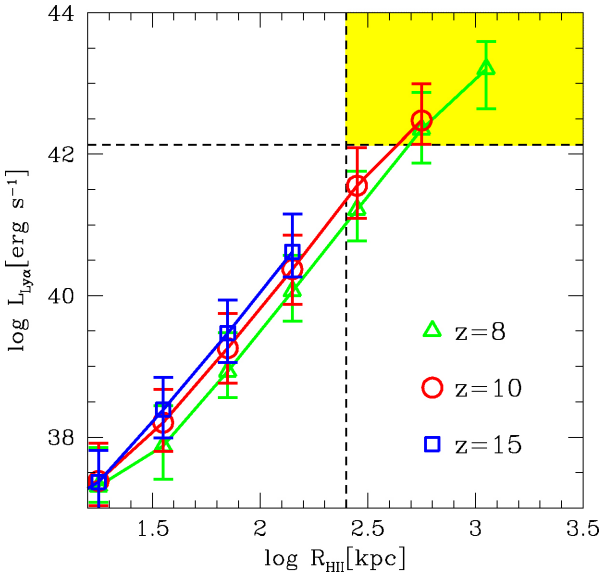

Figure 2: Lyα luminosity as a function of size of HII bubble. Triangle, circle, and square symbols represent median values at z= 8, 10, and 15, respectively. Error bars show quartiles. The horizontal dash line shows the flux for $z = 10$. The vertical dash line represents the viewing angle of 1 arcmin for $z = 10$. Figure extracted from Yajima et al. (2018).

The Yajima model does not assume equilibrium between the number of photoionizations and recombinations and takes into account the evolution of the size of the bubble with time. The model establishes a relation between the observed Lyman alpha line luminosity and the radius of the Strömgren sphere as a function of redshift. This method works because the intrinsic Lyman alpha luminosity depends on the number of ionizing photons according to the following relation

$$L_{Ly\alpha,int}\,[erg/s] = 1.19 \cdot 10^{-11} \cdot Q_{ion} = 1.19 \cdot 10^{-11} \cdot [Q^*_{ion} \cdot (1 - f_{esc,LyC})], \tag{4}$$

where Q_{ion} is the effective number of ionizing continuum photons emitted per second and Q^*_{ion} is the intrinsic number of stellar ionizing continuum photons emitted per second. This is related to the number of ionizing continuum photons emitted per second as

$$\dot{N}_{ion} = Q^*_{ion} \cdot f_{esc,LyC}, \tag{5}$$

where $f_{esc,LyC}$ is the escape fraction from the ionizing continuum, that is the fraction of ionizing continuum photons that manage to escape from the HII region without being absorbed or suffering scattering. In the Yajima model, it is assumed a $f_{esc,LyC} = 0.2$. The same definition, but for the Lyα line, will be introduced later: escape fraction of Lyα photons, $f_{esc,Ly\alpha}$.

It is important not to mislead between $\dot{N}_{ion}$ and Q^*_{ion}. The former represents the number of ionizing continuum photons that actually participate in reionizing the intergalactic medium. The latter represents the rate of ionizing continuum photons directly emitted by the massive (O, B) start, not considering any absorption, scattering, or escape fraction from the nebula without effectively ionizing the gas. On the other hand, Q_{ion} is the rate of ionizing continuum photons that corresponds to the intrinsic Lyα luminosity.

3.3 Sobral relation

To calculate the Strömgren radius using the Yajima method, it is sufficient to know the redshift and the observed Lyα luminosity of our source, since it assumes a fixed value of $f_{esc,Ly\alpha} = 0.6$. However, in the case of the Strömgren radius assuming equilibrium, things get complicated. We need to know the intrinsic number of ionizing photons and for this we have to estimate the Lyman alpha escape fraction.

One way to estimate this parameter is by using the Sobral relation (Sobral, David and Matthee, Jorryt, 2019). This relation links the Lyα escape fraction, $f_{esc,Ly\alpha}$, with the equivalent width in the rest-frame of Lyα, $EW_{rest\,frame}$. Thus, knowing the equivalent width of the Lyα line, the escape fraction can be directly obtained. This relation is given by,

$$f_{esc,Ly\alpha} = 0.0048\,(\pm 0.0007)\cdot EW_{rest\,frame} \pm 0.05 \text{ for } 0 \leq EW_{rest\,frame} \leq 200 \text{ Å}. \tag{6}$$

For $EW_{rest\,frame} > 200$, we will assume that $f_{esc,Ly\alpha} = 1$, meaning all the Lyα emission escapes without being altered. Note that the equivalent width of Lyα, $EW_{rest\,frame}$, is related to the continuum luminosity, L_{1200} by the following definition.

$$EW_{rest\,frame} \equiv \frac{L(Ly\alpha)}{L_{1200}} \tag{7}$$

Besides, this $EW_{rest\,frame}$ is in the rest-frame, meaning it is the intrinsic EW of the emission and does not correspond to the observed one. To obtain the observed equivalent width, simply multiply by $(1+z)$. The Figure 3 illustrates the Sobral relation. Although it has a slight dependence on redshift, it can be assumed to be independent of it due to overlapping uncertainties.

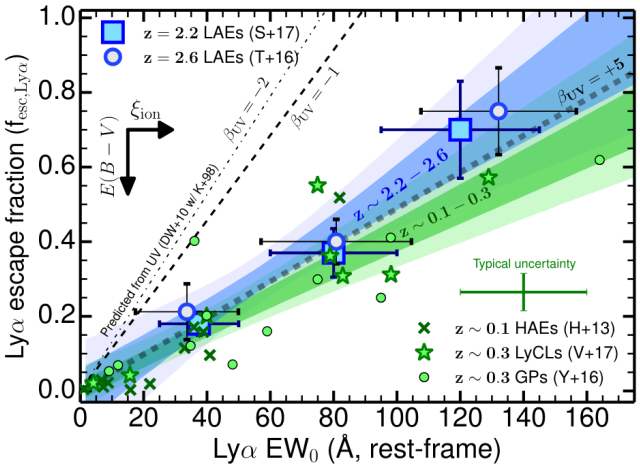

Figure 3: The relation between $f_{\text{esc, Ly}\alpha}$ and Lyα EW$_0$ for $z \sim 2.2$, $z \sim 2.6$ and comparison with $z \sim 0-0.3$ samples. It shows the 1σ and 2σ range for the fits at $z \sim 2.2-2.6$ and $z \sim 0-0.3$ separately, and finds them to be consistent within those uncertainties, albeit with a potential steeper relation at higher redshift. The Sobral relation finds a combined best fitting relation given by $f_{\text{esc, Ly}\alpha} = 0.0048$ EW$_{rest\,frame} \pm 0.05$. Figure extracted from Sobral, David and Matthee, Jorryt (2019).

In conclusion, using the Sobral relation, it will be able to determine the escape fraction of the Lyα photons which, according to its definition given by

$$f_{esc,Ly\alpha} = \frac{L_{Ly\alpha,obs}}{L_{Ly\alpha,int}}, \tag{8}$$

will allow us to determine the number of ionizing photons using the equations 4 and 5. $L_{Ly\alpha,obs}$ and $L_{Ly\alpha,int}$ are the observed and intrinsic luminosity of the Lyα line, respectively.

4 Samples and derived parameters

In this section, we will present all the samples and calculate some of the important parameters obtained in this work. Specifically, we will show the tables of the different galaxy samples we have worked with. These tables will include, in addition to the main parameters, the new ones that have been estimated. It is important to note that the tables that will be displayed in this section will only show some of the columns and rows of interest. Access to the complete tables is available as explained in Appendix A. Additionally, as we discussed the different samples, we will also calculate some important parameters using the given equations previously.

The galaxy samples we work with are extracted from Kerutt et al. (2022), Jung et al. (2019), Hu et al. (2021), Tilvi et al. (2020), Flury et al. (2022), Atek et al. (2024) and Williams et al. (2023). These samples contain LAEs galaxies and their Strömgren radius will be estimated by using the methods explained before.

4.1 Kerutt data

The Kerutt sample, extracted from Kerutt et al. (2022), contains 34 LAEs objects from the MUSE-Wide survey. All these samples have redshift between 3 and 6.5 but the data have been filtered to work only with galaxies with $z > 6$. In Table 1, we display some of the galaxies belonging to the Kerutt sample.

Table 1: LAEs galaxies extracted from Kerutt et al. (2022). The Lyα escape fractions, $f_{esc,Ly\alpha}$, Yajima's Strömgren radii, R_s, and Strömgren radii in equilibrium, R_s^{eq}, are parameters calculated in this research.

ID	z	$EW_{rest\,frame}$ [Å]	$log(L_{Ly\alpha}[erg/s])$	$f_{esc,Ly\alpha}$	R_s^{eq} [pMpc]	R_s [pMpc]
13444244	6.04 ± 0.00	553.37 ± 0.00	42.33 ± 0.41	1.00 ± 0.00	0.50 ± 0.01	0.60 ± 0.12
13464246	6.05 ± 0.01	150.50 ± 0.00	41.82 ± 1.31	0.72 ± 0.00	0.37 ± 0.03	0.43 ± 0.09
13694272	6.10 ± 0.01	88.09 ± 26.45	42.56 ± 0.64	0.42 ± 0.13	0.78 ± 0.03	0.71 ± 0.14
13754278	6.10 ± 0.00	45.39 ± 16.66	42.32 ± 0.81	0.22 ± 0.08	0.81 ± 0.05	0.60 ± 0.12
13774280	6.11 ± 0.01	864.36 ± 0.00	42.53 ± 0.71	1.00 ± 0.00	0.57 ± 0.03	0.69 ± 0.14
13974303	6.24 ± 0.01	105.99 ± 0.00	41.83 ± 1.35	0.51 ± 0.00	0.40 ± 0.03	0.43 ± 0.09
13984304	6.25 ± 0.01	21.71 ± 25.31	41.62 ± 2.65	0.10 ± 0.12	0.58 ± 0.01	0.37 ± 0.08

Note: Explanations of the columns: ID: Identifier from the MUSE-Wide survey. z: Redshift based on the Lyman α line. $EW_{rest\,frame}$: Rest-frame EW in Å. $log(L_{Ly\alpha})$: Observed Lyα luminosity in dex units of ergs per second. $f_{esc,Ly\alpha}$: Escape fraction of Lyα photons. R_s^{eq}: Strömgren radius assuming equilibrium in $pMpc$. R_s: Strömgren radius calculated by the Yajima method in $pMpc$.

The Lyα escape fractions, $f_{esc,Ly\alpha}$, Yajima's Strömgren radii, R_s, and Strömgren radii in equilibrium, R_s^{eq}, from the Kerutt data, Table 1, are parameters calculated in this research. The rest of them were extracted from the publication.

As we will see with the rest of the samples, one of the first steps is to calculate the Lyα photon escape fraction, $f_{esc,Ly\alpha}$. Given the equivalent width, $EW_{rest\,frame}$, it is easy to estimate this parameter using the Sobral relation (equation 6). Once obtained, using equation 8, the intrinsic Lyα luminosity is obtained. Finally, with all these parameters calculated, it is possible to estimate the Strömgren radius assuming equilibrium (equation 3) using equations 4 and 5. For this process, and the rest of the work, we will assume a $f_{esc,LyC} = 0.2$, because of the reasons presented in Yajima et al. (2018). In contrast, to obtain the Strömgren radius using Yajima's method, we have simply employed Yajima's model (Figure 2).

4.2 Jung, Hu, and Tilvi data

The Jung, Hu, and Tilvi samples were extracted from Jung et al. (2019), Hu et al. (2021), and Tilvi et al. (2020), respectively. The Jung data correspond to a sample of 15 LAEs galaxies extracted from the Texas Spectroscopy Search. These objects were detected using the Keck/MOSFIRE instrument of the W. M. Keck Observatory. On the other hand, the 21 LAEs galaxies presented in the Hu data correspond to the protocluster LAGER-z7OD1 at a redshift of 6.93. This protocluster belongs to the Lyman Alpha Galaxies in the Epoch of Reionization (LAGER) survey and was studied using the Cerro Tololo Inter-American Observatory (CTIO) Blanco 4m telescope. This protocluster will be important for the conclusions since is the only sample of grouped galaxies that we have. Finally, the 3 LAEs galaxies of the Tilvi data belong to the DAWN survey and were measured using the Kitt Peak 4m Mayall telescope. In Tables 2, 3, and 4 we display some of the galaxies belonging to the Jung, Hu, and Tilvi samples, respectively.

Table 2: LAEs galaxies extracted from Jung et al. (2019). The Lyα escape fractions, $f_{esc,Ly\alpha}$, and the equilibrium Strömgren radius, R_s^{eq}, are parameters calculated in this study.

ID	z	$EW_{rest\,frame}$ [Å]	$log(L_{Ly\alpha}[erg/s])$	$f_{esc,Ly\alpha}$	R_s^{eq} [pMpc]	R_s [pMpc]
z7_GND_44088	7.13 ± 0.00	$87.60^{+23.80}_{-21.20}$	42.90 ± 0.20	$0.42^{+0.11}_{-0.10}$	$0.78^{+0.03}_{-0.03}$	0.88 ± 0.00
z8_GND_22233	7.34 ± 0.00	$54.50^{+15.00}_{-12.10}$	42.96 ± 0.16	$0.26^{+0.07}_{-0.06}$	$0.91^{+0.05}_{-0.05}$	0.92 ± 0.00
z7_GND_18626	7.42 ± 0.00	$26.80^{+14.90}_{-9.80}$	42.26 ± 0.22	$0.13^{+0.07}_{-0.05}$	$0.66^{+0.10}_{-0.10}$	0.52 ± 0.00
z7_GND_42912	7.51 ± 0.00	$33.20^{+4.30}_{-4.00}$	43.01 ± 0.09	$0.16^{+0.02}_{-0.02}$	$1.08^{+0.05}_{-0.05}$	0.96 ± 0.00
z7_GND_6330	7.55 ± 0.00	$15.90^{+4.40}_{-3.70}$	42.46 ± 0.17	$0.08^{+0.02}_{-0.02}$	$0.90^{+0.17}_{-0.17}$	0.62 ± 0.00
z7_GND_16863	7.60 ± 0.00	$61.30^{+14.40}_{-11.40}$	43.13 ± 0.10	$0.29^{+0.07}_{-0.06}$	$0.95^{+0.03}_{-0.03}$	1.07 ± 0.00
z7_GND_34204	7.61 ± 0.00	$279.70^{+80.40}_{-62.50}$	43.51 ± 0.13	$1.00^{+0.00}_{-0.30}$	$0.84^{+0.01}_{-0.01}$	1.44 ± 0.00

Note: Explanations of the columns: ID: Identifier from the Texas Spectroscopic Search. z: Redshift based on the Lyman α line. $EW_{rest\,frame}$: Rest-frame EW in Å. $log(L_{Ly\alpha})$: Observed Lyα luminosity in dex units of ergs per second. $f_{esc,Ly\alpha}$: Escape fraction of Lyα photons. R_s^{eq}: Strömgren radius assuming equilibrium in $pMpc$. R_s: Strömgren radius calculated by the Yajima method in $pMpc$.

Table 3: LAEs galaxies extracted from Hu et al. (2021). The Lyα escape fractions, $f_{esc,Ly\alpha}$, and the equilibrium Strömgren radius, R_s^{eq}, are parameters calculated in this study.

ID	z	$EW_{rest\,frame}$ [Å]	$log(L_{Ly\alpha}[erg/s])$	$f_{esc,Ly\alpha}$	R_s^{eq} [pMpc]	R_s [pMpc]
LAE-1	6.94 ± 0.00	89.63 ± 0.00	$43.54^{+0.03}_{-0.03}$	0.43 ± 0.00	$1.32^{+0.01}_{-0.01}$	1.83 ± 0.00
LAE-2	6.93 ± 0.00	26.33 ± 0.00	$43.33^{+0.07}_{-0.08}$	0.13 ± 0.00	$1.70^{+0.08}_{-0.09}$	1.45 ± 0.00
LAE-3	6.92 ± 0.00	71.86 ± 0.00	$43.49^{+0.04}_{-0.05}$	0.34 ± 0.00	$1.38^{+0.02}_{-0.01}$	1.73 ± 0.00
LAE-4	6.90 ± 0.00	79.52 ± 0.00	$43.04^{+0.09}_{-0.11}$	0.38 ± 0.00	$0.95^{+0.02}_{-0.02}$	1.08 ± 0.00
LAE-5	6.90 ± 0.00	93.00 ± 0.00	$43.03^{+0.07}_{-0.08}$	0.45 ± 0.00	$0.89^{+0.01}_{-0.01}$	1.01 ± 0.00
LAE-6	6.92 ± 0.00	81.00 ± 0.00	$43.03^{+0.10}_{-0.14}$	0.39 ± 0.00	$0.93^{+0.02}_{-0.03}$	0.92 ± 0.00
LAE-7	6.95 ± 0.00	32.54 ± 0.00	$42.79^{+0.12}_{-0.17}$	0.16 ± 0.00	$1.04^{+0.07}_{-0.10}$	0.77 ± 0.00

Note: Explanations of the columns: ID: Identifier from the LAGER survey. z: Redshift based on the Lyman α line. $EW_{rest\,frame}$: Rest-frame EW in Å. $log(L_{Ly\alpha})$: Observed Lyα luminosity in dex units of ergs per second. $f_{esc,Ly\alpha}$: Escape fraction of Lyα photons. R_s^{eq}: Strömgren radius assuming equilibrium in $pMpc$. R_s: Strömgren radius calculated by the Yajima method in $pMpc$.

Table 4: LAEs galaxies extracted from Tilvi et al. (2020). The Lyα escape fractions, $f_{esc,Ly\alpha}$, and the equilibrium Strömgren radius, R_s^{eq}, are parameters calculated in this study.

ID	z	$EW_{rest\,frame}$ [Å]	$log(L_{Ly\alpha}[erg/s])$	$f_{esc,Ly\alpha}$	R_s^{eq} [pMpc]	R_s [pMpc]
z8_SM	7.77 ± 0.00	23 ± 6	42.30 ± 0.5	0.11 ± 0.03	0.67 ± 0.25	0.55 ± 0.00
z8_4	7.75 ± 0.00	71 ± 18	42.60 ± 0.25	0.34 ± 0.09	0.58 ± 0.04	0.69 ± 0.00
z8_5	7.73 ± 0.00	37 ± 3	43.08 ± 0.08	0.18 ± 0.01	1.04 ± 0.04	1.02 ± 0.00

Note: Explanations of the columns: ID: Identifier from the DAWN survey. z: Redshift based on the Lyman α line. $EW_{rest\,frame}$: Rest-frame EW in Å. $log(L_{Ly\alpha})$: Observed Lyα luminosity in dex units of ergs per second. $f_{esc,Ly\alpha}$: Escape fraction of Lyα photons. R_s^{eq}: Strömgren radius assuming equilibrium in $pMpc$. R_s: Strömgren radius calculated by the Yajima method in $pMpc$.

For Jung, Hu, and Tilvi data, the Lyα escape fractions, $f_{esc,Ly\alpha}$ and Strömgren radii in equilibrium, R_s^{eq}, are parameters calculated in this research. The procedure followed to obtain these parameters has been the same as that used for Kerutt data, namely, using equations 3, 4, 5, 6, and 8. The rest of the parameters, including in this case the Strömgren radii calculated using Yajima's method, R_s, were extracted from the publications.

4.3 Flury data

Flury data represent a different sample from the others presented in this project as they are low-redshift LAEs galaxies. Therefore, we will limit ourselves to estimating their Lyman alpha photon escape fraction, $f_{esc,Ly\alpha}$. Flury data correspond to 66 LAEs galaxies from the Low-redshift Lyman Continuum Survey (LzLCS), detected with the Hubble Space Telescope (HST). In Table 5, we display some of the galaxies belonging to the Flury sample.

Table 5: LAEs galaxies extracted from Flury et al. (2022). The Lyα escape fraction, $f_{esc,Ly\alpha}$, has been calculated in this study.

ID	z	$EW_{rest\,frame}$ [Å]	$log(L_{Ly\alpha}[erg/s])$	$f_{esc,Ly\alpha}$
J003601+003307	0.35 ± 0.00	93.90 ± 9.33	$42.13^{+0.05}_{-0.05}$	0.45 ± 0.05
J004743+015440	0.35 ± 0.00	41.53 ± 4.43	$42.57^{+0.05}_{-0.05}$	0.20 ± 0.02
J011309+000223	0.31 ± 0.00	31.29 ± 3.56	$42.30^{+0.05}_{-0.05}$	0.15 ± 0.02
J012217+052044	0.37 ± 0.00	70.62 ± 6.80	$42.60^{+0.04}_{-0.04}$	0.34 ± 0.03
J012910+145935	0.28 ± 0.00	39.59 ± 4.84	$42.48^{+0.06}_{-0.05}$	0.19 ± 0.02
J072326+414608	0.30 ± 0.00	49.99 ± 4.42	$42.30^{+0.05}_{-0.04}$	0.24 ± 0.02
J080425+472607	0.36 ± 0.00	233.68 ± 20.57	$42.46^{+0.04}_{-0.04}$	1.00 ± 0.00

Note: Explanations of the columns: ID: Identifier from the LzLCS survey. z: Redshift based on the Lyα line. $EW_{rest\,frame}$: Rest-frame EW in Å. $log(L_{Ly\alpha})$: Observed Lyα luminosity in dex units of ergs per second. $f_{esc,Ly\alpha}$: Escape fraction of Lyα photons.

To estimate the Lyα photon escape fraction, $f_{esc,Ly\alpha}$, for the Flury sample, the same procedure already explained has been followed, using the Sobral relation (equation 6).

4.4 JWST data

The method for detecting distant galaxies using gravitational lenses is based on the ability of massive objects, such as galaxy clusters, to bend the light passing near them, acting as a natural lens. This phenomenon, known as gravitational lensing, magnifies and distorts the light from galaxies located behind the massive object from the perspective of Earth. By observing these distortions and magnifications, we can identify and study galaxies that would otherwise be too faint. In this subsection, we present distant galaxies detected using this method.

First of all, the Atek data shown in Table 7, extracted from Atek et al. (2024), pertain to galaxies detected thanks to the gravitational lens Abell 2744 (A2744). On the other hand, we present a galaxy at redshift 9.5 extracted from the article by Williams et al. (2023). This galaxy was detected thanks to another gravitational lens known as RX J2129, and its data are collected in Table 6. This latest galaxy will help us to understand the evolution of ionization bubbles, as it is the most distant galaxy presented in this work. In Tables 6 and 7, we display the Williams and Atek samples, respectively.

Table 6: Distant galaxy extracted from Williams et al. (2023). The equilibrium Strömgren radius, R_s^{eq}, has been calculated in this study.

ID	z	$log(M/M_\odot)$	SFR $[M_\odot/yr]$	$12+log(O/H)$	R_s^{eq} [pMpc]
RX- J2129-z95	9.51 ± 0.01	$7.63^{+0.22}_{-0.24}$	$1.69^{+0.51}_{-0.34}$	$7.48^{+0.07}_{-0.05}$	$0.39^{+0.04}_{-0.03}$

Note: Explanations of the columns: ID: Identifier for the object in Abell 2744 gravitational lens. z: Spectroscopic redshift. $log(M/M_\odot)$: Logarithm of stellar mass in dex units. SFR: Estimation of Star Formation Rate using Hα emission in solar masses per year. $12+log(O/H)$: Oxygen abundance. R_s^{eq}: Strömgren radius assuming equilibrium in $pMpc$.

Table 7: Distant galaxies extracted from Atek et al. (2024). The equilibrium Strömgren radius, R_s^{eq}, has been calculated in this study.

ID	z	$log(M/M_\odot)$	SFR $[M_\odot/yr]$	$12+log(0/H)$	R_s^{eq} [pMpc]
18924	7.70 ± 0.00	$5.88^{+0.13}_{-0.08}$	0.33 ± 0.02	6.95 ± 0.15	0.33 ± 0.01
16155	6.87 ± 0.00	$6.61^{+0.07}_{-0.06}$	0.92 ± 0.04	7.01 ± 0.19	0.56 ± 0.01
23920	6.00 ± 0.00	$6.30^{+0.03}_{-0.03}$	1.32 ± 0.04	6.84 ± 0.06	0.79 ± 0.01
12899	6.88 ± 0.00	$6.54^{+0.14}_{-0.19}$	0.49 ± 0.02	6.70 ± 0.15	0.45 ± 0.01
8613	6.38 ± 0.00	$7.12^{+0.07}_{-0.08}$	0.78 ± 0.07	6.97 ± 0.18	0.60 ± 0.02
23619	6.72 ± 0.00	$6.57^{+0.10}_{-0.06}$	0.85 ± 0.07	7.19 ± 0.20	0.57 ± 0.02
38335	6.23 ± 0.00	$6.83^{+0.25}_{-0.20}$	1.00 ± 0.16	7.46 ± 0.32	0.68 ± 0.04

Note: Explanations of the columns: ID: Identifier for each source used in Atek et al. (2024). z: Spectroscopic redshift. $log(M/M_\odot)$: Logarithm of stellar mass in dex units. SFR: Estimation of Star Formation Rate using Hα emission in solar masses per year. $12+log(O/H)$: Oxygen abundance. R_s^{eq}: Strömgren radius assuming equilibrium in $pMpc$.

The Strömgren radius assuming equilibrium, R_s^{eq}, is a parameter calculated in this research for these two samples. The rest of them were extracted from the corresponding publication. The Strömgren radius using Yajima's method, R_s, was not calculated because we did not have data on the Lyα line for the samples preventing us from using it.

To calculate R_s^{eq}, we did the following. Thanks to the data collected by the JWST telescope, we have been able to work with the Hα recombination line instead of Lyα. Given the star formation rates, SFR, as shown in Tables 6 and 7, we can determine the Hα luminosity and, consequently, the number of ionizing continuum photons emitted per second according to the following expressions Kennicutt (1983), Williams et al. (2023).

$$SFR[M_\odot/yr] = 5.5 \cdot 10^{-42} \cdot L(H\alpha)[erg/s] \tag{9}$$

and

$$L(H\alpha)[erg/s] = 1.36 \cdot (1 - f_{esc,LyC}) \cdot 10^{-12} \cdot \dot{N}_{ion}[s^{-1}]. \tag{10}$$

Therefore, knowing the number of ionizing photons, the Strömgren radius assuming equilibrium is directly calculated using equation 3.

5 Results

In this section, we will present and analyze the results obtained primarily for the escape fractions and the Strömgren radii calculated for some of the studied samples. Specifically, we will compare different models and analyze their differences.

5.1 Escape fraction

This subsection aims to compare the values calculated in Section 4 for the escape fraction of Lyα photons, $f_{esc,Ly\alpha}$, with those provided by stellar spectral energy distribution (SED) synthesis models. Specifically,

we will use the escape fractions calculated for the samples from Kerutt and Flury data (Subsections 4.1 and 4.3) and compare them with the predictions of the models done by Cerviño et al. (2002).

The SED model that we are going to apply assumes a metallicity of Z = 0.008 - 0.020, an Instantaneous Burst (IB) or Continuous Star Formation Rate (CSFR) model, and a Salpeter Initial Mass Function (IMF) with a coefficient of $\alpha = 2.35$. Additionally, we will omit the existence of binary systems and assume a stellar and nebular component with a filling factor (ff) equal to unity. All these assumptions will lead to negligible degeneracies. For more information about this SED stellar model, consult the Appendix B.

The applied SED models do not directly predict escape fractions; however, we can estimate them using their predictions. To do this, we extract from the models the values of the luminosity in the continuum per unit mass, $\mathscr{L}_{1285}$, and the number of ionizing photons per unit mass, $Q(H^0)$, for a certain age. Thus, by simply applying the expressions,

$$\frac{L_{1200}\,[\mathrm{erg}\cdot\mathrm{s}^{-1}\cdot\mathrm{\AA}^{-1}]}{\mathscr{L}_{1285}\,[\mathrm{erg}\cdot\mathrm{s}^{-1}\cdot\mathrm{\AA}^{-1}\cdot M_{\odot}^{-1}]} = M\,[M_{\odot}] \tag{11}$$

and,

$$M[M_{\odot}]\cdot Q(H^0)[photons\cdot s^{-1}\cdot M_{\odot}^{-1}] = \dot{N}_{ion}^{model}[photons\cdot s^{-1}], \tag{12}$$

we obtain the number of ionizing photons predicted by the model, $\dot{N}_{ion}^{model}$. Consequently, using equations 4, 5 and 8, along with the observed Lyα luminosity of the sample, we directly obtain the Lyα photon escape fraction predicted by the model, $f_{esc,Ly\alpha}^{model}$.

With all this information, we can now compare the Lyα photon escape fractions obtained using the SED model, with those obtained in Section 4 for the data from Kerutt and Flury (Subsections 4.1 and 4.3). This comparison is carried out for different conditions in terms of $\mathscr{L}_{1285}$, $Q(H^0)$, and age. In Figure 4 we present these results for both samples.

One might expect a one-to-one relation in Figure 4. However, this is not the case because, depending on the physical conditions of the medium ($\mathscr{L}_{1285}$, $Q(H^0)$, and age), the escape fraction obtained using the SED models can vary significantly. Therefore, we observe a cone shape, indicating the range of values within which the actual Lyα photon escape fraction can fluctuate. Note that since the differences and errors in the escape fractions are significant (a mean relative error of 30%), the values in the Strömgren radius we will obtain in the next section will be estimations. This is one of the, for now, consequences of studying the Lyα line at high redshift with current technology.

On the other hand, Figure 4 can also be understood as a comparison between the estimated escape fraction based on the Sobral relation, $f_{esc,Ly\alpha}$, and the estimation from the models, $f_{esc,Ly\alpha}^{model}$. With this, one could estimate which physical conditions are closer to the Sobral relation. Finally, it should be noted that the error bars in Figure 4 have been calculated by error propagation. The errors in Kerutt data are much larger than those in Flury data simply because the former has errors in the Lyα luminosity of a greater order of magnitude.

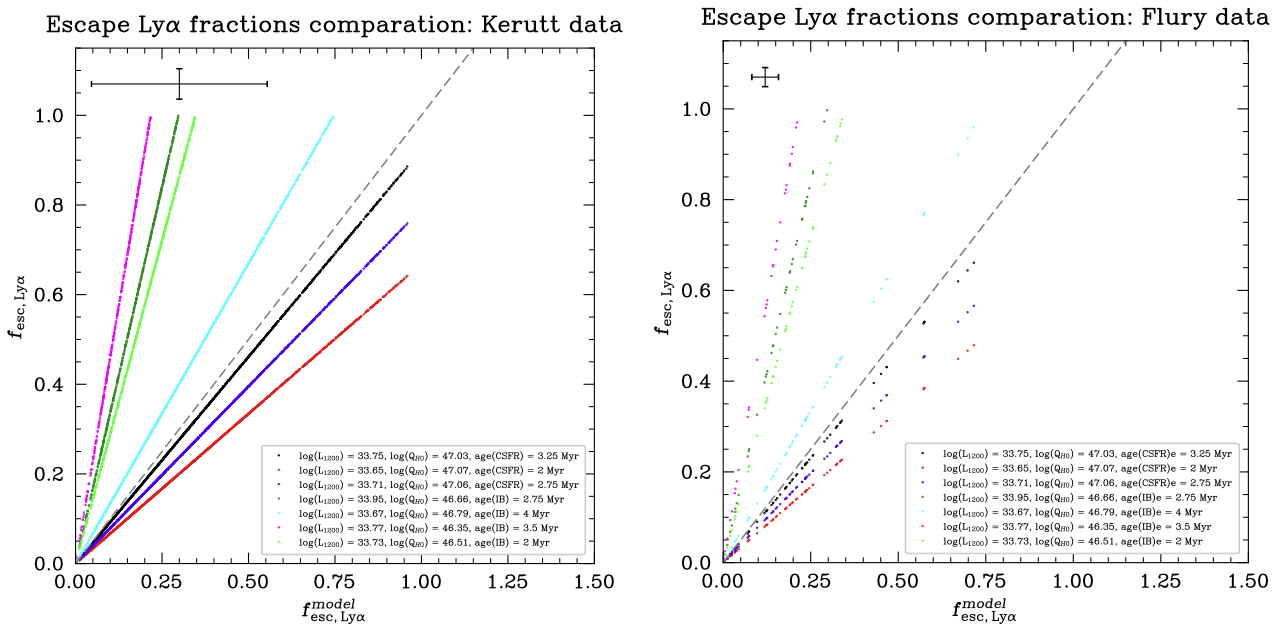

Figure 4: Lyα escape fractions calculated from the Kerutt sample (left; Section 4.1) and Flury sample (right; Section 4.3) as a function of the escape fraction obtained from (Cerviño et al., 2002) SED models for different conditions in $\mathscr{L}_{1285}$, $Q(H^0)$, and age. The dashed gray line indicates the ideal one-to-one relation, which implicates that most galaxies must be experiencing star formation processes between ages of 3 Myr and 4 Myr. The abbreviations IB and CSFR in the age part of the legend correspond to Instantaneous Burst and Continuous Star Formation Rate models, respectively. A 'cone' shape is observed rather than a one-to-one relation, indicating the range of values the escape fraction can vary due to the physical conditions of the medium. The error bars represent the median of the errors calculated by propagation. Galaxies with $f_{esc,Ly\alpha} = 1$ have been omitted.

Finally, in view of Figure 4, the Instantaneous Burst (IB) model at 4 Myr and the Continuous Star Formation Rate (CSFR) model at 3.25 Myr are the ones that best approximate Sobral's prediction (closer to the one-to-one relation), which is empirical. Therefore, most galaxies must be experiencing star formation processes between ages of 3 Myr and 4 Myr.

5.2 Strömgren radius

At this moment, it is time to recap one of the most important results of this project: the estimation of the size of the reionized bubbles around each star-forming galaxy.

As we did in Section 4, using Equation 3, and other equations to estimate the number of ionizing photons (Equations 4, 5, 6 and 8), we estimated the size of the ionization bubbles assuming equilibrium surrounding our high redshift galaxies. Figure 5 shows two histograms (one for all the samples and the other separating them) depicting the sizes of these ionized bubbles for all samples, except for Flury data due to its low redshift (the Universe was fully reionized by then).

All calculated Strömgren radii exceed the minimum limit of $R_s^{eq} = 0.3\ pMpc$. This limit, estimated by Mason and Gronke (2020), represents the minimum radius the ionized bubble should have for Lyα emission to escape the bubble without being absorbed due to the Hubble flow. The ionizing bubble is large enough to allow the Lyα emission to expand sufficiently to avoid its absorption upon exiting it. However,

this limit serves as a lower limit for extreme cases, i.e., for very particular physical conditions. This limit typically lies around $R_s^{eq} = 0.5\ pMpc$.

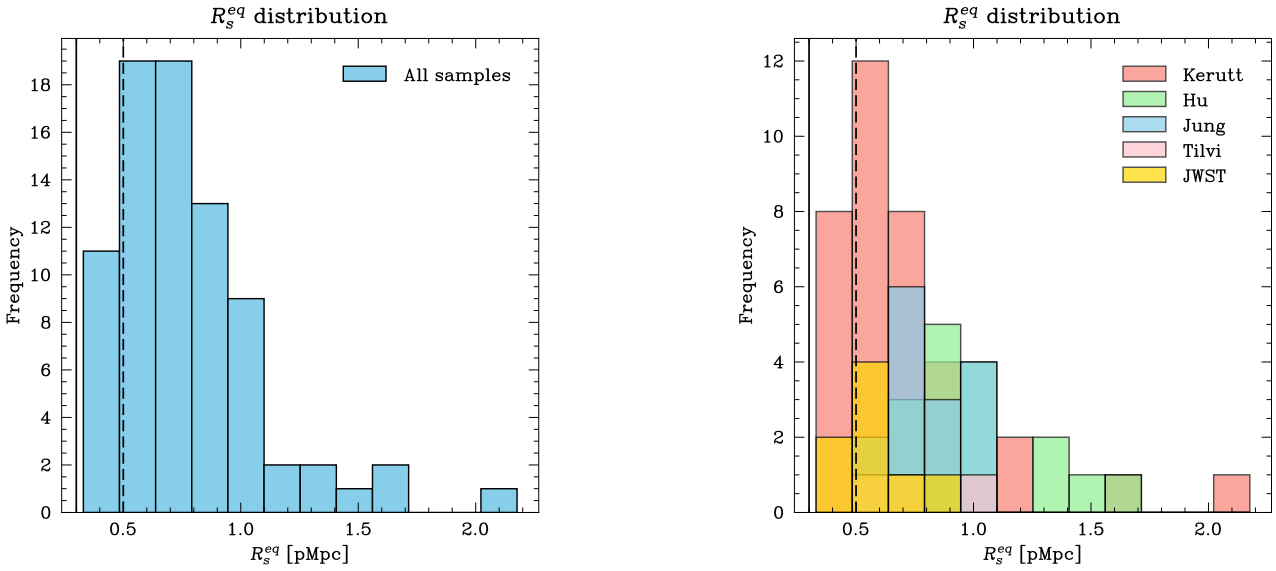

Figure 5: Distribution of the Strömgren radius calculated for all samples combined (left) and separately (right). A peak is observed around $R_s^{eq} \simeq 0.7\ pMpc$, with all galaxies surpassing the minimum limit in the size of the ionized bubble for detecting Lyα. The dashed line represents the approximate limit ($R_s^{eq} \simeq 0.5\ pMpc$) for detecting Ly$\alpha$, while the solid line represents the minimum limit ($R_s^{eq} \simeq 0.3\ pMpc$) for detecting Ly$\alpha$ for extreme cases (Mason and Gronke, 2020).

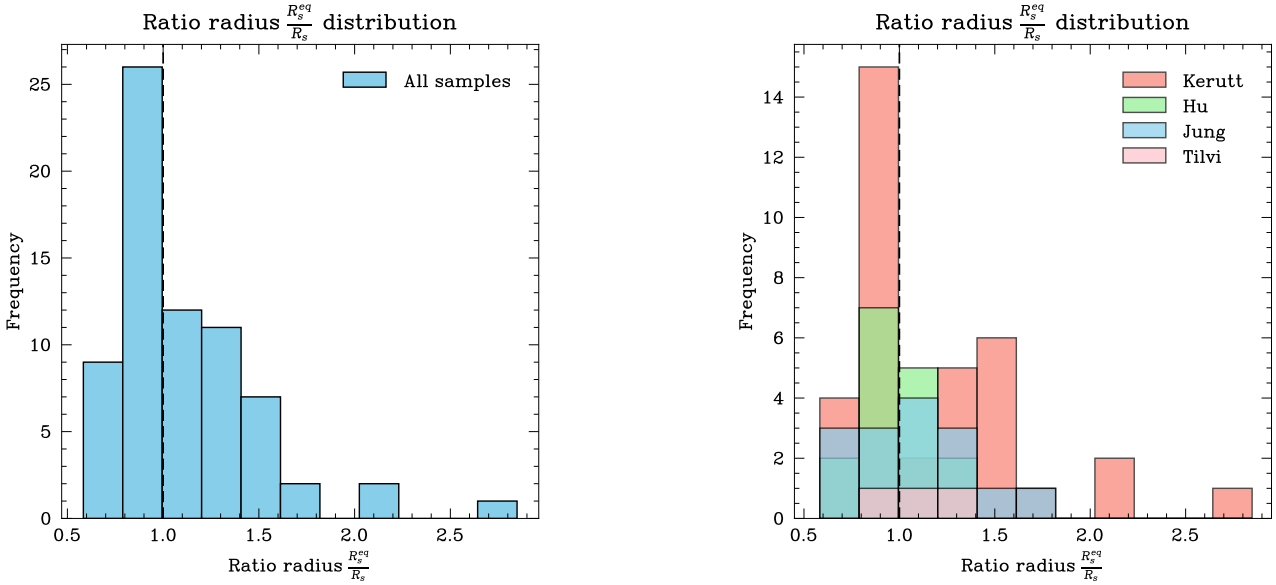

Figure 6: Distribution of the ratio between the Strömgren radius calculated assuming equilibrium and the one calculated by the Yajima model, R_s^{eq}/R_s, for all the sample (left) and separately (right). The majority of the values (80% in 1-σ region) are clustered around $R_s^{eq}/R_s \sim 1$ (dashed vertical line), indicating that the assumption of equilibrium is not far from reality. The distribution shows a small tail towards higher values of the R_s^{eq} due to its upper bound.

The results we have shown are assuming equilibrium between ionizations and recombinations. However, it is worth investigating whether this assumption is correct or not. One way to check this is by taking the ratio between the Strömgren radius assuming equilibrium, R_s^{eq}, and the one obtained by the Yajima model, R_s (remembering that the latter did not assume equilibrium and took into account the evolution over time). Figure 6 shows this procedure in the form of a histogram for the Kerutt, Hu, Jung, and Tilvi samples, while we omit samples that do not have Lyα emission measures (Atek and Williams data) or the sample was at low redshift (Flury data).

The majority of galaxies exhibit a ratio $R_s^{eq}/R_s \sim 1$. However, the distribution shows a small tail towards higher values of the Strömgren equilibrium radius. This implies that Equation 3 provides an upper bound on the estimation of the Strömgren radius. Nevertheless, 80% of the galaxies lie within the 1-σ region, indicating that assuming equilibrium, while representing an upper bound, serves as a reasonable first approximation.

5.3 Comparison between methods

Finally, in this results section, we will present some scale relations that have been found between the various parameters we have worked with and estimated. These scaling relationships will allow us to compare in even more detail the two methods used to estimate the Strömgren radius: assuming equilibrium (Equation 3) or by Yajima (Figure 2). Firstly, we are going to analyze the $f_{esc,Ly\alpha}$ relation.

In Yajima's model, a fixed value of $f_{esc,Ly\alpha} = 0.6$ is assumed. This assumption has significant implications: when the actual value of $f_{esc,Ly\alpha}$ is less than 0.6, the correction to obtain the $Ly\alpha$ luminosity is greater. Consequently, the estimated equilibrium radius, R_s^{eq}, also increases proportionally. Then, when the values of $f_{esc,Ly\alpha}$ diverge significantly from the assumed value of 0.6, the R_s^{eq} value is more representative of the actual observations.

This is a weak point of Yajima's model. It would be ideal to develop a model similar to Yajima's but incorporating Sobral's equation to use a correct value of $f_{esc,Ly\alpha}$. By doing so, a more accurate estimation of the intrinsic $Ly\alpha$ luminosity can be obtained, which in turn would provide a more precise calculation of the equilibrium radius. Figure 7 illustrates this behavior.

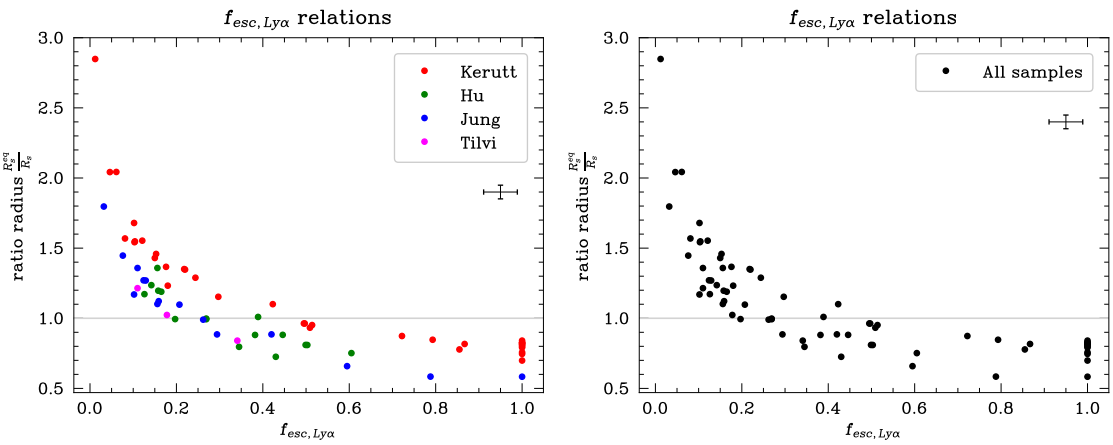

Figure 7: Relation between R_s^{eq}/R_s and escape fraction of Lyα photons, $f_{esc,Ly\alpha}$ for all the samples (right) and separately (left). For very low $f_{esc,Ly\alpha}$, both methods seem to diverge, while at high $f_{esc,Ly\alpha}$, they converge to $R_s^{eq}/R_s \sim 1$, with a small error of 20% (probably derived from assumptions). This is because, at low $f_{esc,Ly\alpha}$ values, the upper bound marked by the Strömgren radius assuming equilibrium increases

On the other hand, when a galaxy has a very low equivalent width, $EW_{rest\,frame}$, the R_s^{eq}/R_s ratio diverges. This is because the escape fraction estimated by Sobral's equation (Equation 6) diverges from the one assumed by Yajima ($f_{esc,Ly\alpha} = 0.6$), resulting in an underestimation of the radius with Sobral's method. However, for larger $EW_{rest\,frame}$, this R_s^{eq}/R_s relation converges to unity (with a 20% error derived from the assumptions made), demonstrating that both methods return the same value. In the Figure 8 we show this scale relation.

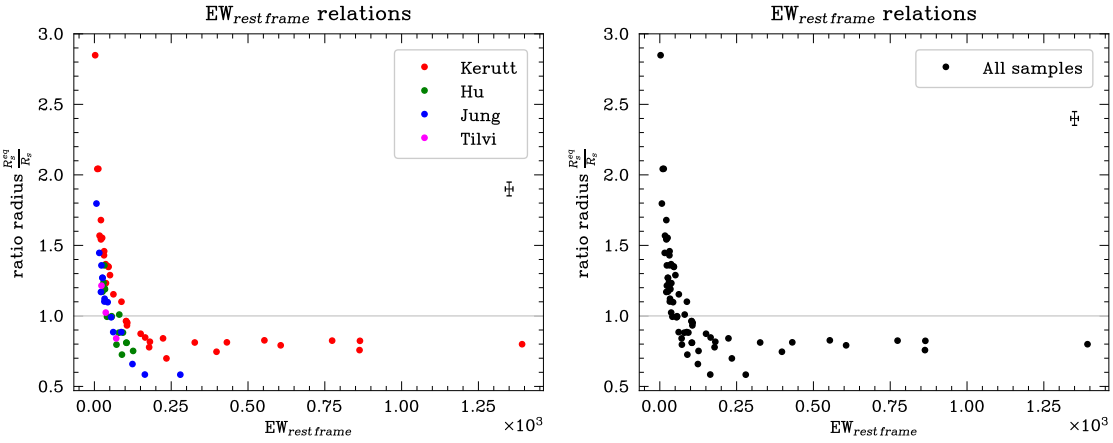

Figure 8: Relation between R_s^{eq}/R_s and equivalent width of Lyα in the rest frame, $EW_{rest\,frame}$ for all the samples (right) and separately (left). For very low $EW_{rest\,frame}$, both methods seem to diverge, while at high $EW_{rest\,frame}$, they converge to $R_s^{eq}/R_s \sim 1$, with a small error of 20% (probably derived from assumptions). This is because, at low $EW_{rest\,frame}$ values, the upper bound marked by the Strömgren radius assuming equilibrium increases.

Finally, one of the most compelling relations that allows us to assess the goodness of the Yajima model compared to assuming equilibrium is shown in Figure 9. At high redshifts, when the Universe was still undergoing reionization, the R_s^{eq}/R_s ratio yields values less than unity, suggesting that the Strömgren radius calculated assuming equilibrium is incorrect. Therefore, at these redshifts, it is preferable to use the Yajima method since it accounts for the temporal scale. However, as the reionization epoch comes to an end, the R_s^{eq}/R_s ratio converges as equilibrium between ionizations and recombinations is reached. Thus, the Yajima method becomes unnecessary, and assuming equilibrium is a good approximation. These results are shown in Figure 9, where we have assumed a $f_{esc,Ly\alpha} = 0.6$ for the calculation of R_s^{eq}.

Note that, although at high redshifts the Strömgren radius in equilibrium may not seem realistic, it can be assumed as a first approximation since the errors in the observed and derived parameters are generally much larger than 30%.

Finally, it should be mentioned that the estimated Strömgren radii for the high-redshift galaxies from the Atek and Williams data (Subsection 4.4) are small. That is, they are close to the limit values for detecting Lyα predicted by Mason and Gronke (2020). Since these Strömgren radii, calculated assuming equilibrium, represent an upper bound for high-redshift galaxies, the results are consistent with the fact that Lyα emission has not been detected for these two samples.

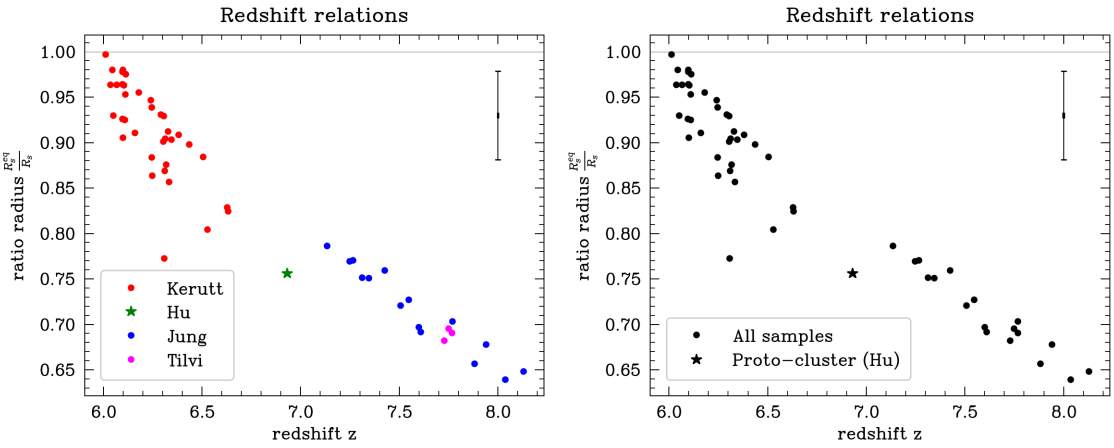

Figure 9: Relation between R_s^{eq}/R_s and redshift, z, assuming $f_{esc,Ly\alpha} = 0.6$ for the calculation of R_s^{eq} for all the samples (right) and separately (left). The green star refers to the proto-cluster LAGER-z7OD, meaning we have treated all the galaxies as one. At high z, it is not appropriate to assume equilibrium since the ionization and recombination processes are still very active. As we approach $z \sim 6$, at the end of the reionization epoch, equilibrium is reached, and the Yajima method becomes unnecessary.

6 Summary and conclusions

The study of ionization bubbles during the epoch of reionization stands as one of the focal points in current astrophysics. Its examination is of paramount importance for comprehending the processes of stellar formation in galaxies at high redshifts.

In this study, various samples extracted from Kerutt et al. (2022), Hu et al. (2021), Jung et al. (2019), Flury et al. (2022), Tilvi et al. (2020), Williams et al. (2023), Atek et al. (2024), primarily comprising Lyα Emitters (LAEs) at high redshifts, have been employed to estimate their Lyα photon escape fractions and assess the size of their ionization bubbles. When a galaxy at high redshift emits in the Ultra-Violet (UV) photons at 912 Å, a portion of its emission will be attenuated by the presence of HI regions. This phenomenon arises because, in the early stages of the primitive Universe, the intergalactic medium was not yet fully ionized, hindering the transmission of the total UV emission from these objects. Understanding the intrinsic emission of these sources is crucial for studying the properties of such high-redshift objects.

One of the main studied parameters was the escape fraction of Lyα photons, $f_{esc,Ly\alpha}$. These estimated escape fractions have been compared with those predicted by SED models (Subsection 5.1). This comparison has ensured the accuracy of our escape fraction estimates and indicates that most galaxies must be experiencing star formation processes between 3 and 4 Myr. Nevertheless, this remains a highly significant parameter that is conditioned by the physical conditions of the medium, as depicted in Figure 4. On the other hand, the Strömgren radii of the ionized bubbles have been estimated (Figures 5 and 6). Two methods have been employed for this purpose: one assuming equilibrium between the number of ionizations and recombinations, R_s^{eq} (Subsection 3.1), and the other considering the temporal scale, R_s (Subsection 3.2), termed the Yajima model. The estimated sizes of the ionization bubbles align with the results predicted in the literature (Mason and Gronke, 2020), exceeding the minimum possible radii predicted. This justifies the detection of Lyα emission from the studied galaxies, as their bubbles were sufficiently large to be detected due to the Hubble flow and the fact that the galaxies on which Hα was observed, but not Lyα, show ionized radii generally low.

To consolidate all our estimations of these parameters and methods, we have identified some scale relations of interest among different parameters (Subsection 5.3). These relations have enabled us to conclude that, although assuming equilibrium between recombinations and photoionizations at high redshifts may entail some inaccuracies, it serves as a reasonable initial approximation for estimating the size of these bubbles with errors of up to 30%, with errors becoming negligible when approaching $z \sim 6$ (Figure 9). However, when dealing with higher redshifts, applying the Yajima model provides a more robust estimation of the size of these bubbles. On the other hand, the fact that Yajima model assumes a constant value of $f_{esc,Ly\alpha}$ is an important caveat.

Lastly, it is noteworthy to mention the galaxy RX-J2129-z95 at z$\sim$ 9.5, from Williams data, for which one of the smallest Strömgren radii obtained in this project is detected (Subsection 4.4). The Strömgren radius of this high-redshift galaxy has been calculated using the equilibrium relation, thus representing an upper limit to its size. Even being an upper limit, the radius we have derived is very close to the minimum limit predicted by Mason and Gronke (2020), and well below the standard value of 0.5 $pMpc$, thus justifying the non-detection of Lyα emission

The study of the epoch of reionization represents a field of vital importance for understanding the processes of formation and evolution of the first stars and galaxies in the Universe. Thanks to new instruments such as the JWST, this field continues to be nourished by knowledge and will yield new results.

Appendix A: Complete tables and programmed code

All the programming notebooks for this work are available on GitHub at https://github.com/juananmcl/Internship_CAB/tree/main, covering parameter estimation, error calculation, figure generation, and more, including all necessary data and complete Tables 1 - 6. Accessing and running these notebooks is recommended for a comprehensive understanding.

Appendix B: SED stellar models

The Spectral Energy Distribution (SED) stellar models employed are those programmed by various authors and collected at https://cab.inta-csic.es/users/mcs/SED2/sed.php?op1=01. We acknowledge Cerviño et al. (2002) as one of the latest contributors to the model's code, whom we consult when using it. For information on the physical foundation and operation of these models, please refer to the provided link.

References

Atek, H., Labbé, I., Furtak, L. J., Chemerynska, I., Fujimoto, S., Setton, D. J., Miller, T. B., Oesch, P., Bezanson, R., Price, S. H., Dayal, P., Zitrin, A., Kokorev, V., Weaver, J. R., Brammer, G., Dokkum, P. v., Williams, C. C., Cutler, S. E., Feldmann, R., Fudamoto, Y., Greene, J. E., Leja, J., Maseda, M. V., Muzzin, A., Pan, R., Papovich, C., Nelson, E. J., Nanayakkara, T., Stark, D. P., Stefanon, M., Suess, K. A., Wang, B., and Whitaker, K. E. (2024). Most of the photons that reionized the Universe came from dwarf galaxies. *nat*, 626(8001):975–978.

Cen, R. and Haiman, Z. (2000). Quasar strömgren spheres before cosmological reionization. *The Astrophysical Journal*, 542(2):L75.

Cerviño, M., Mas-Hesse, J. M., and Kunth, D. (2002). Evolutionary synthesis models of starbursts. IV. Soft X-ray emission. *AAP*, 392:19–31.

Flury, S. R., Jaskot, A. E., Ferguson, H. C., Worseck, G., Makan, K., Chisholm, J., Saldana-Lopez, A., Schaerer, D., McCandliss, S., Wang, B., Ford, N. M., Heckman, T., Ji, Z., Giavalisco, M., Amorin, R., Atek, H., Blaizot, J., Borthakur, S., Carr, C., Castellano, M., Cristiani, S., De Barros, S., Dickinson, M., Finkelstein, S. L., Fleming, B., Fontanot, F., Garel, T., Grazian, A., Hayes, M., Henry, A., Mauerhofer, V., Micheva, G., Oey, M. S., Ostlin, G., Papovich, C., Pentericci, L., Ravindranath, S., Rosdahl, J., Rutkowski, M., Santini, P., Scarlata, C., Teplitz, H., Thuan, T., Trebitsch, M., Vanzella, E., Verhamme, A., and Xu, X. (2022). The Low-redshift Lyman Continuum Survey. I. New, Diverse Local Lyman Continuum Emitters. *apjs*, 260(1):1.

Gazagnes, S., Chisholm, J., Schaerer, D., Verhamme, A., and Izotov, Y. (2020). The origin of the escape of Lyman α and ionizing photons in Lyman continuum emitters. *AAP*, 639:A85.

Hayes, M., Schaerer, D., Östlin, G., Mas-Hesse, J. M., Atek, H., and Kunth, D. (2011). On the Redshift Evolution of the Lyα Escape Fraction and the Dust Content of Galaxies. *APJ*, 730(1):8.

Hu, W., Wang, J., Infante, L., Rhoads, J. E., Zheng, Z.-Y., Yang, H., Malhotra, S., Barrientos, L. F., Jiang, C., González-López, J., Prieto, G., Perez, L. A., Hibon, P., Galaz, G., Coughlin, A., Harish, S., Kong, X., Kang, W., Khostovan, A. A., Pharo, J., Valdes, F., Wold, I., Walker, A. R., and Zheng, X. (2021). A Lyman-α protocluster at redshift 6.9. *Nature Astronomy*, 5:485–490.

Jung, I., Finkelstein, S. L., Dickinson, M., Hutchison, T. A., Larson, R. L., Papovich, C., Pentericci, L., Song, M., Ferguson, H. C., Guo, Y., Malhotra, S., Mobasher, B., Rhoads, J., Tilvi, V., and Wold, I. (2019). Texas Spectroscopic Search for Lyα Emission at the End of Reionization. II. The Deepest Near-infrared Spectroscopic Observation at z $\gtrsim$ 7. *apj*, 877(2):146.

Kennicutt, R.C., J. (1983). The rate of star formation in normal disk galaxies. *APJ*, 272:54–67.

Kerutt, J., Wisotzki, L., Verhamme, A., Schmidt, K. B., Leclercq, F., Herenz, E. C., Urrutia, T., Garel, T., Hashimoto, T., Maseda, M., Matthee, J., Kusakabe, H., Schaye, J., Richard, J., Guiderdoni, B., Mauerhofer, V., Nanayakkara, T., and Vitte, E. (2022). Equivalent widths of Lyman α emitters in MUSE-Wide and MUSE-Deep. *aap*, 659:A183.

Madau, P. (1995). Radiative Transfer in a Clumpy Universe: The Colors of High-Redshift Galaxies. *APJ*, 441:18.

Mas-Hesse, J. M., Kunth, D., Tenorio-Tagle, G., Leitherer, C., Terlevich, R. J., and Terlevich, E. (2003). Lyα Emission in Starbursts: Implications for Galaxies at High Redshift. *APJ*, 598(2):858–877.

Mason, C. A. and Gronke, M. (2020). Measuring the properties of reionized bubbles with resolved Lyα spectra. *MNRAS*, 499(1):1395–1405.

Osterbrock, D. E. (1989). Active galactic nuclei. *Annals of the New York Academy of Sciences*, 571:99–109.

Pentericci, L., Grazian, A., Fontana, A., Castellano, M., Giallongo, E., Salimbeni, S., and Santini, P. (2009). The physical properties of Lyα emitting galaxies: not just primeval galaxies? *AAP*, 494(2):553–561.

Robertson, B. E., Ellis, R. S., Dunlop, J. S., McLure, R. J., and Stark, D. P. (2010). Early star-forming galaxies and the reionization of the universe. *Nature*, 468(7320):49–55.

Rodríguez Espinosa, J., Mas-Hesse, J., Salvador-Solé, E., and Manrique, A. (2021). On the radius of ionised bubbles. *Monthly Notices of the Royal Astronomical Society*, 000:1–3. Preprint.

Sobral, David and Matthee, Jorryt (2019). Predicting ly alpha escape fractions with a simple observable - ly alpha in emission as an empirically calibrated star formation rate indicator. *Asrtonomy and Astrophysics*, 623:A157.

Spitzer, L. (1978). *Physical processes in the interstellar medium*. Spitzer.

Strömgren, B. (1939). The Physical State of Interstellar Hydrogen. *apj*, 89:526.

Tilvi, V., Malhotra, S., Rhoads, J. E., Coughlin, A., Zheng, Z., Finkelstein, S. L., Veilleux, S., Mobasher, B., Wang, J., Probst, R., Swaters, R., Hibon, P., Joshi, B., Zabl, J., Jiang, T., Pharo, J., and Yang, H. (2020). Onset of Cosmic Reionization: Evidence of an Ionized Bubble Merely 680 Myr after the Big Bang. *apjl*, 891(1):L10.

Williams, H., Kelly, P. L., Chen, W., Brammer, G., Zitrin, A., Treu, T., Scarlata, C., Koekemoer, A. M., Oguri, M., Lin, Y.-H., Diego, J. M., Nonino, M., Hjorth, J., Langeroodi, D., Broadhurst, T., Rogers, N., Perez-Fournon, I., Foley, R. J., Jha, S., Filippenko, A. V., Strolger, L., Pierel, J., Poidevin, F., and Yang, L. (2023). A magnified compact galaxy at redshift 9.51 with strong nebular emission lines. *Science*, 380(6643):416–420.

Yajima, H., Sugimura, K., and Hasegawa, K. (2018). Modelling of Lyman-alpha emitting galaxies and ionized bubbles at the epoch of reionization. *Monthly Notices of the Royal Astronomical Society*, 477(4):5406–5421.